On the dynamical coupling between atmospheric blocks and heavy precipitation events: A discussion of the southern Alpine flood in October 2000

Sina Lenggenhager*[1,2], Mischa Croci-Maspoli[3], Stefan Brönnimann[1,2], Olivia Martius[1,2]

[1]Institute of Geography, University of Bern

[2]Oeschger Center for Climate Change Research, University of Bern

[3]Federal Office of Meteorology and Climatology MeteoSwiss, Zürich

*corresponding author: sina.lenggenhager@giub.unibe.ch

Abstract

In October 2000, a high-impact lake flood event occurred in southern Switzerland. During the month prior to the flood event three heavy precipitation events (HPEs) occurred. The first two events preconditioned the catchment and brought the lake close to its flood level. During the third event the lake level rose above the flood threshold. At the same time, anomalously high blocking activity was observed in the northern North-Atlantic/European region. This study describes the synoptic development during the month prior to the flood and investigate the role of atmospheric blocking for the formation of the HPEs using ERA-Interim data. Atmos-

This article has been accepted for publication and undergone full peer review but has not been through the copyediting, typesetting, pagination and proofreading process, which may lead to differences between this version and the Version of Record. Please cite this article as doi: 10.1002/qj.3449

pheric blocks are identified as persistent negative potential vorticity (PV) anomalies in the upper troposphere.

All three heavy precipitation events were forced by upper-level equatorward elongated streams of stratospheric high-PV air (PV streamers). These PV streamers formed in the strong deformation field upstream and downstream of single blocks or in between two blocks. During the third and most persistent heavy precipitation episode the eastward propagation of the PV streamer was prevented by a downstream block for several days leading to a stationary upper-level north-eastward flow and a prolonged period of heavy precipitation over the catchment. The study identifies and quantifies a potential feedback between heavy precipitation and blocks via diabatic depletion of PV. It is shown that a substantial fraction of the diabatically modified low PV air (63%) that reached and strengthened the blocks over the Atlantic and Europe during this month experienced heating in HPE areas.

Keywords: Atmospheric blocking, rainfall, floods, mid-latitude, extra-tropical weather systems, troposphere, dynamic/processes, Switzerland

1 Introduction

Atmospheric blocks are quasi-stationary high-pressure systems. They persist between several days and several weeks. They are characterized by upper-level negative potential vorticity (PV) anomalies in the central blocked region (Pelly and Hoskins 2003; Schwierz et al. 2004; Small et al. 2014). Due to their longevity and stationarity they can play an important role in the formation of surface weather extremes (e.g., Sillmann and Croci-Maspoli, 2009). Blocks can be associated with both anomalously hot and cold temperature extremes (e.g., Sillmann et al, 2011). Clear sky conditions in a summer blocking lead to shortwave radiative heating that can contribute to heat waves (e.g., Sillmann and Croci-Maspoli 2009; Dole et al. 2011; Pfahl and Wernli 2012a) and, depending on the location of the block, the advection of cold, continental air along the eastern flank of a block can lead to cold extremes in winter (e.g., Lackmann et al. 1997; Dole et al. 2011; Pfahl and Wernli 2012b; Bieli et al. 2015; Whan et al. 2016).

Blocking not only affects surface temperature but also precipitation. A relationship between blocks and precipitation patterns was first described by Rex (1950, 1951). He noticed a decrease in precipitation in the central blocked region and a slight precipitation increase along the flanks of the blocks. Changes in precipitation during blocks have been attributed primarily to the effect of the block on cyclone tracks. For example during winter, blocking over central Europe leads to a shift in the cyclone tracks towards the south with a decrease in cyclone frequency over northern Europe and this results in an increase in the mean precipitation rate over southern Europe and a decrease over large parts of north-western Europe (Trigo et al. 2004). Sousa et al. (2017) postulate a general increase of precipitation south of the blocked regions and a decrease in the region of the blocks. These spatial patterns have been confirmed for many locations around the world including the Iberian Peninsula (Sousa et al. 2016), Europe in general (Yao and Luo 2014), and South America (Rodrigues et al. 2017; Fernandes and

Rodrigues 2017). Furthermore, there are indications that the same spatial patterns also apply to extreme precipitation. A climatological study by Carrera et al. (2004) related an increase of precipitation extremes in the south-eastern and the south-western US during winter to Alaskan blocking episodes. A stronger storm track equatorward of the block leads to enhanced moisture transport into California (Carrera et al. 2004).

However, for floods, the link with blocks is more complex as compared to precipitation alone because the temporal evolution of precipitation is important for the formation of flood events. Numerous case studies indicate that floods in Asia (Samel and Liang 2003; Hong et al. 2011; Martius et al. 2013; Antokhina et al. 2018), North America (Milrad et al. 2015), and Europe (Stucki et al. 2012; Grams et al. 2014; Piaget et al. 2015; Barton et al. 2016) can be associated with blocking.

Several dynamical mechanisms have been postulated that link atmospheric blocking and floods. First, blocking can contribute to setting up of synoptic-scale flow patterns that that are known to be associated with extreme precipitation and flooding (Stucki et al. 2012; Martius et al. 2013; Grams et al. 2014; Piaget et al. 2015; Milrad et al. 2015; Barton et al. 2016). This entails meridional flow amplification, Rossby wave breaking, and cut-off formation upstream or downstream of a block. The diffluent flow upstream of a block assists the meridional amplification of synoptic-scale eddies (e.g., Shutts 1983) but also anticyclonic Rossby wave breaking downstream of blocks is frequent (Altenhoff et al. 2008).

Second, blocking may modulate the frequency and duration of precipitation leading to flooding. This includes flood preconditioning via increased mean precipitation on sub-seasonal and seasonal time scales upstream or equatorward of a blocked area that will increase the susceptibility to flooding (e.g., Jacobeit et al. 2006, see also previous discussion). In addition, blocking can affect the flood-triggering precipitation. For example, blocking has further been related to recurring extreme precipitation events over the same area, which are instrumental for

flood formation (Hong et al. 2011; Lau and Kim 2012; Martius et al. 2013; Yamada et al. 2016).

In addition, there is potentially a two-way interaction between blocking and heavy precipitation via latent heating during the formation of heavy precipitation. As established recently, latent heating plays an important role in the formation and maintenance of blocking via upper-level depletion of PV that feeds into the negative PV anomaly of the block (Massacand et al. 2001; Croci-Maspoli and Davies 2009; Pfahl et al. 2015). Heavy precipitation events (HPEs) associated with flooding might enforce downstream blocking via diabatic PV depletion. While links between heavy precipitation and blocks have been previously discussed, to our knowledge, a systematic analysis and summarizing discussion of the complex dynamical links between floods and blocks is so far missing.

Here, we present a detailed analysis of links between blocking and a flood event by studying one of the most damaging flood events in southern Switzerland in recent decades. This flood occurred as consequence of three HPEs in the catchment area within less than a month (Barton et al. 2016). HPEs on the southern side of the Alps are typically associated with upper-level equatorward elongated streams of stratospheric high-PV air over western Europe, so-called PV streamers (Massacand et al. 1998; Fehlmann et al. 2000; Froidevaux and Martius 2016; Martius et al. 2006). These upper-level PV streamers are associated with reduced static stability underneath and the advection of moist and warm air from the south toward the Alps. These moist air masses then undergo orographic and quasi-geostrophic lifting (e.g., Martius et al. 2006; Pfahl et al. 2014). The combined effects can contribute to the formation of heavy to extreme precipitation.

The overall aim of this study is to disentangle, describe, and document the multitude of the dry and moist dynamical processes that link atmospheric blocking, heavy precipitation, and flooding for one case of severe flooding in southern Switzerland. In addition, we address the question if a feedback via diabatic processes between extreme precipitation events and associ-

ated blocking can be established by using back-trajectories starting from the blocks and forward trajectories started from areas of heavy precipitation.

The paper is organised as follows. In section 2 the data and methods, specifically the trajectory calculations, are described. Section 3 motivates and introduces the selected case study. Section 4 provides a synoptic overview of the flood event, which is followed by a detailed discussion of the involved dry and moist dynamical processes in section 5. A summary and discussion of the different processes follows in section 6. The paper closes with conclusions in section 7.

2 Data and Methods

2.1 Data

All our analyses are based on the ERA-Interim reanalysis data (Dee et al. 2011) by the European Center for Medium-Range Weather Forecasts (ECMWF). All fields are horizontally interpolated to a regular 1° by 1° grid. The data is available on 60 vertical levels with a temporal resolution of six hours. The dataset covers the period since 1979 and is extended in real time. In our analyses, we use data from 1979 to 2015.

Heavy precipitation events (HPEs) are defined using the ERA-Interim precipitation data. This has the advantage of a dynamically consistent dataset. ERA-Interim precipitation stems from short-term forecasts and while ERA-Interim data generally underestimates the absolute values of precipitation, the timing of extreme precipitation in the extra-tropics is quite well represented (Pfahl and Wernli 2012a). Accordingly, we are primarily interested in the occurrence of HPEs, not their magnitude. All precipitation fields have a spin-up time of at least 6 hours. The precipitation fields were summed up to daily accumulations (from 2100 UTC of the day before to 2100 UTC). Every day with precipitation exceeding the 95^{th} all-year percentile is considered a HPE. No temporal de-clustering was performed.

A basic quality assessment of the ERA-Interim precipitation for September and October 2000 is provided through a comparison with two independent rain-gauge based gridded precipitation datasets. First, we use the European dataset E-OBS (Haylock et al. 2008) that provides daily precipitation accumulations based on station data and covers the 1950-2006 period with a spatial grid resolution of 0.5° by 0.5°. Second, we employ the Swiss dataset RhiresD (Frei and Schär 1998; MeteoSwiss 2016) provided by the Federal Office of Meteorology and Climatology (MeteoSwiss) for the overview of the temporal evolution of the precipitation in the Lago-Maggiore catchment. It provides daily precipitation accumulations since 1961. The spa-

tial grid resolution is 1 km. Due to its high spatial resolution, it is assumed to be more accurate for the precipitation in the complex topography around the Lago Maggiore than the coarser resolved E-OBS data. The daily accumulation period is from 0600 UTC until 0600 UTC the next day. The catchment-aggregated data was taken from Barton et al. (2015). The lake level data for the Lago Maggiore measured in Locarno was provided by the Swiss Federal Office for the Environment.

2.2 Tools and Methods

Here, blocks are defined as persistent negative PV anomalies in the upper troposphere following Pfahl and Wernli (2012b), in a slight adaptation of the method introduced by Schwierz et al. (2004). First, vertically averaged PV (VAPV) anomalies, between 500 hPa and 150 hPa, are determined. The anomalies are taken to a 30-day running mean climatology for 1979-2015. Then, anomalies are masked by using two thresholds: -1.0 pvu (weak blocks) and -1.3 pvu (strong blocks). To be considered as blocks, these negative anomalies need to persist for at least five days and need to have a spatial overlap between two time steps of at least 70% of the area. To identify the blocks uniquely, they were labelled with numbers. When two blocks merge, the merged block obtains the label of the older block.

To analyse the link between precipitation extremes, diabatic heating and blocks, we use a trajectory approach similar to that of Pfahl et al. (2015). Lagrangian back trajectories are calculated with the LAGRANTO2.0 tool (Wernli and Davies 1997; Sprenger and Wernli 2015). Trajectories are started from 8 pressure levels (500 hPa to 150 hPa, every 50 hPa) at every longitude / latitude grid point within the horizontal extent of strong blocks where the PV is <= 2 pvu in the region 120° W-120° E/0° N-90° N between 15 September 2000, 0000 UTC and 15 October 2000, 1800 UTC. The grid points are the same at every level, however, stratospheric air with PV above 2 pvu is excluded. The positions of the parcels trajectories are calculated 72 h back in time and several atmospheric parameters (PV, potential temperature,

relative and absolute humidity) are tracked along the flow. We chose a 72-hours for the following reasons. The time window needs to be long enough to capture air parcels that undergo diabatic heating and ascend from the lower troposphere to the upper troposphere. Some of this ascent might happen in warm conveyor belts in the warm sector of cyclones upstream or south of a block. In a warm conveyor belts the ascent happens within 48-hours (Wernli and Davies 1997, Schemm et al. 2013, Madonna et al. 2014). However, we do not want to restrict the analysis only to WCB trajectories and therefore use a longer time window.

For the subsequent statistics, we select the trajectories with PV values of less than 2 pvu at their starting location to only catch tropospheric air parcels. The total number of back trajectories is 586'753.

A second set of trajectories is calculated starting from HPE areas going 72 hours forward in time. We start the trajectories at all grid points inside the HPEs (daily precipitation above the 95th percentile, see section 2.1) on 15 pressure levels between 850 hPa and 150 hPa in 50 hPa steps (constrained to the region 120° W-120° E/30° N-90° N). For subsequent analyses, only the air parcels with a relative humidity of more than 80% are selected, which likely contribute to precipitation formation. The total number of forward trajectories is 284'813.

We define all forward and backward trajectories that experience a diabatic heating of at least 5 K during the 72-hour period as the group of strongly diabatically influenced air parcels. The difference in potential temperature is taken between the maximum and the minimum at any time step before the maximum. All the statistical trajectory analyses presented are area-weighted with the cosine of the latitude of their starting location.

3 The October 2000 floods south of the Alps and in the UK

We study the flooding of Lago Maggiore, a lake located on the southern edge of the Swiss Alps, in the second half of October 2000. Precipitation during the entire month prior to the flood event was above normal. The monthly precipitation accumulation between 15 September and 15 October 2000 over the western parts and south of the Alps exceeded the local 95th monthly percentile (Figure 1a and b). The precipitation accumulation of ERA-Interim (Figure 1b) for the period from 15 September to 15 October 2000 generally agrees well with precipitation accumulation of E-OBS (Figure 1a), however, the absolute precipitation south of the Alps is lower in ERA-Interim compared to E-OBS. The relative precipitation is also smaller in ERA-Interim, the precipitation accumulation exceeded the local 95th monthly percentile only at one grid point over the Alps.

In the month prior to the flood, three extreme precipitation events occurred in the Lago Maggiore catchment (Figure 2, see also Barton et al. 2015). The first one occurred on 20 September 2000, the second one on 30 September 2000, and the third one from 11 October 2000 to 15 October 2000. Concomitantly, the level of Lago Maggiore rose successively (Figure 2). During the third precipitation event with the largest precipitation accumulation (see also Lawrimore et al. 2001; Gabella and Mantonvani 2001) the lake flooded the surroundings. Between the extreme precipitation episodes, the lake level never returned to its initial level (Figure 2). The daily lake level rates during the first, second and third event was up to 8, 9 and 13 standard deviations, respectively (not shown). This evolution of the lake level suggests that without the first two extreme precipitation events the lake level would not have reached such high levels during the third precipitation event and thus all three events contributed to the flood.

Barton et al. (2015) provide a detailed discussion of the local upper-level dynamics associated with these HPEs. They show that each of the three HPEs was heralded by the formation of a

meridionally elongated upper-level high PV trough, i.e. PV streamer, over western Europe and associated very high to extreme moisture transport towards the Alps from the south. Quasi-geostrophic and orographic lifting of these moist air masses resulted in the HPEs.

Lago Maggiore was not the only place subject to heavy precipitation and floods in this period. In the south-eastern UK flooding started after heavy precipitation from 11 to 13 October following a wet September (Saunders et al. 2001).

4 Synoptic Overview

4.1 Upstream flow over the Atlantic sector prior to 20 September 2000

On 16 September 2000, a block (B1) formed over the western North-Atlantic (Figure 3a) and on 17 September it merged with a second block further north into one large block extending from 50° N to 75° N and 60° W to 30° W (Figure 3b, c). At the western flank of B1 heavy precipitation was present throughout 16, 17, and 18 September (Figure 3a, b, c, d). The precipitation was associated with a strong extratropical cyclone over north-eastern Canada (Figure 4a) that had previously merged with former hurricane Florence during the latter's extratropical transition. Back trajectories, that are started on 20 September 1800 UTC at vertically every 50 hPa between 500 hPa and 150 hPa and horizontally at every grid point in the region of the block B1 and that experienced strong (>5K) diabatic heating and were almost saturated (>80%) while they passed a HPE region, i.e. were associated with a HPE (for details see section 2.2), indicate that the air has moved upward and equatorward along the western flank of the block. During the rising, the air that experienced latent heating, which resulted in cross-isentropic transport of low-PV air from the lower to the upper troposphere (for more details see section 5.4). This low-PV air ended up in B1 two days later over the eastern Atlantic and hence contributed to a strengthening of this block (Figure 4a, b).

From 16 September to 18 September a weak block was present over Scandinavia (B2) (Figure 3a-e) that became a strong block on 19 September (Figure 3e). An upper-level high PV trough located in the deformation flow field between the two blocks B1 and B2, amplified meridionally between 17 and 19 September 2000 and formed a PV streamer, while B1 was growing, amplifying and moving eastward (Figure 3c-e). On 19 September at 0600 UTC the streamer's eastern flank was located over the European Atlantic coast and heavy precipitation occurred over Portugal, the Bretagne, central France, south-eastern UK, and the south-western coast of

Norway (Figure 3e) which was likely facilitated by quasi-geostrophic lifting associated with the upper-level PV streamer. During 19 September the southern part of the PV streamer cut off of the main stratospheric PV pool (Figure 3f). On 20 September, B1 moved further east and merged with B2 (Figure 3g, h). Back trajectories from block B1 on 20 September 18 UTC suggest that diabatic heating contributed to the block's low PV anomaly and the erosion of the poleward connection of the PV streamer to the main stratospheric air mass and the merging of blocks B1 and B2 (Figure 4b).

At the same time the cut-off streamer's eastern flank reached Switzerland and led to the first HPE (see also Barton et al. 2016). 72-hour back trajectories starting from B1 on 22 September 1800 UTC (see Figure 3i) indicate that the air that was lifted along the Alpine south side, precipitated and experienced latent heat release on 20 September and ended in B1 two days later contributing to the negative PV anomaly of the block (Figure 4c, d). In total, 21% and 8% of the air masses in B1 on 22 September experienced moderate (>2K) and strong (>5K) latent heating, respectively, in the preceding 72h. Of these, 21% and 44%, respectively, originated from a HPE region.

4.2 Upstream flow over the Atlantic prior to the second event on 30 September 2000

On 22 September 2000, a strong North-Atlantic block (B3) had formed almost at the same location as B1 eight days before (Figure 5a). At same time the extratropical transition of a tropical cyclone (TC) Gordon took place. The ex-TC located at 65° W and 60° N merged with a pre-existing extratropical low around 725° W and 60° N at 1200 UTC 22 September (Figure 5a) and this low-pressure system was associated with heavy precipitation (Figure 5a and 6a). Back trajectories starting from B3 on 24 September 1200 UTC (Figure 6b) show that this block was influenced by the intense latent heating related to heavy precipitation associated

with the extratropical system (38% of the block was heated more than 5K). The northerly branch of the trajectories was associated with a warm conveyor belt (not shown). The specific contribution of ex-Gordon to the latent heating is not quantified. Subsequently, B3 amplified, expanded zonally, and moved slowly north-eastward over the following four days (Figure 5b, c, d). B1 was still located over Scandinavia but was weakening and turned into a weak block on 23 September 2000 (Figure 5b). B3 and B1 merged on 25 September (Figure 5d). A cyclonically breaking wave formed upstream of B1 on 24 September and 27 September (Figure 5c) and resulted in a zonal flow over the western Atlantic.

On 25 September, former TC Helen was located south of Cape Hatteras and merged with a weak extratropical low over Cape Hatteras (not shown). Over the course of the following few days this merged low pressure system deepened and moved further east over the North Atlantic (not shown). At upper levels this system was associated with a small ridge downstream (centered approximately at 45°W and 50°N in Figure 5d and at 35°W and 50°N in Figure 5e). Subsequent cyclonic wave breaking upstream of this ridge over the following days led to a zonally elongated PV streamer over the western Atlantic on 27 September (Figure 5f). On 28 September, the upstream wave train intensified and the PV streamer started wrapping up cyclonically over the eastern Atlantic and the UK (Figure 5g). The HPE extending across France and the UK is associated with a WCB (not shown). On 29 September 0000 UTC ex-TC Helen was located over England (not shown) and the meridional elongation of the upper-level high PV blob over western Europe between a ridge over the central Atlantic and the B1 over Scandinavia started (Figure 5h). Heavy precipitation occurred over France. On 30 September, heavy precipitation occurred south of the Alps and the PV streamer over western Europe extended equatorward all the way to North Africa.

4.3 Upstream flow over the Atlantic prior to the third event on 11 to 15 October 2000

Between 30 September and 5 October, the weak B1 moved slowly north-eastward (not shown). Thereafter B1 remained quasi-stationary over western Russia and became a strong block again (Figure 7a). Several anticyclonic wave-breaking events occurred downstream of B1 over the Eurasian continent (Figure 7a, b). On 11 October at 1200 UTC B1 extended over large parts of Siberia and the eastern flank of a broad high PV trough reached western Europe (Figure 7b). At the surface a strong, quasi-stationary low pressure system was situated over the UK (Figure 8a) that was associated with a prolonged period of precipitation in this region. The low-level west-south-westerly flow associated with the upper-level trough brought humid air towards the Alps (Barton et al., 2016) and extreme precipitation started (Figure 8a). The precipitation was extreme in the observations as well as in ERA-Interim (Figure 7b, c, d). Over the western Atlantic a pronounced ridge was present that classified as a weak block (B4, Figure 7c, d). While the precipitation in Switzerland continued (Figure 7e, f, g, h, i and 8a, c), the trough over western Europe was slowly being stretched meridionally between a downstream ridge and the eastward moving B4 upstream (Figure 7c, d, e). On 12 October at 1200 UTC B4 disappeared and a weak block (B5) formed in the downstream ridge at 20° E and 50° N. This block intensified and became a strong block on 13 October at 0000 UTC (Figure 7e, f). The PV streamer over western Europe was further elongated on 13 and 14 October (Figure 7f, g) and a cut-off formed on 14 October (Figure 7h). At this point, the block and the cut-off formed a clear Rex-Block configuration, which helped to keep the system stationary (see Altenhoff et al., 2009 for details about the process). On 15 October the cut-off remained quasi-stationary over the Mediterranean. Precipitation in southern Switzerland was extreme in both the observations and ERA-Interim between 11 and 15 October.

B5 contributed to the meridional stretching of the trough over western Europe. Back trajectories from B5 and B1 starting on 13 October 1200 UTC show that latent heating associated

with extreme precipitation over large parts of western Europe two days earlier contributed to the low PV anomalies of B1 (Figure 8a, b) and latent heating associated with extreme precipitation over the north-western Atlantic probably contributed to the low PV anomaly of B5. Back trajectories starting from B1 and B5 on 14 October 1200 UTC show that latent heating associated with extreme precipitation over Scandinavia as well as over southern Switzerland two days earlier contributed to low PV anomaly of B1 and that the latent heating over the north-western Atlantic contributed to B5.

5. The role of latent heating connected to heavy precipitation for the blocks

In the previous section, we showed that a block was present downstream of the Alps during all three HPEs and that this block and the blocks upstream over the Atlantic were instrumental for setting up the synoptic-scale flow associated with the HPEs. Given the results from Pfahl et al. (2015), who showed the importance of diabatic processes upstream of blocks for the maintenance of these blocks, we looked at the fraction of air parcels experiencing latent heating (and associated upper-level diabatic PV depletion) reaching the blocks over Europe and the Atlantic during our case study. In accordance with Pfahl et al. (2015) we find that between 15 September and 15 October a portion of the blocking air masses in the Euro-Atlantic region experienced diabatic heating. Of all the air masses reaching the blocks, 27% (39%) experienced a strong (moderate) diabatic heating during the 72 hours before their arrival in the block (Figure 9). These numbers are smaller than the climatological mean of 46% that Pfahl et al. (2015) postulated. A reason for the smaller numbers could be that we chose a threshold of 2 pvu to separate the tropospheric from the stratospheric air masses, while Pfahl et al. (2015) used a 1 pvu threshold.

Of these strongly (moderately) diabatically heated air masses, the fraction that pass a HPE region while being almost saturated (>80% RH) at least once in the 72 h is 63% (46%). We assume that quasi-saturated air parcels passing a HPE area experience lifting, contribute to the heavy precipitation and hence experience diabatic heating. This is confirmed by heating centred composites that show that the air parcels experience maximum diabatic heating when they are over the HPE areas (not shown). These fractions reduce to 34% (24%) when using a 99^{th} percentile threshold to identify the HPEs instead of the 95^{th} percentile.

The daily fraction of diabatically heated air parcels that cross heavy precipitation areas varies between 0% and 80% between 15 September and 15 October (Figure 10), but is overall rela-

tively constant with a standard deviation of +-16%. In other words, roughly two thirds of the air parcels that experience latent heating before entering a block, cross an area of heavy precipitation when they are almost saturated, suggesting a strong link between extreme precipitation and the upper-level low PV anomalies of blocks through the latent heat release in ascending air streams.

To illustrate the complexity of the link between diabatic heating associated with heavy precipitation and blocks we show a detailed analysis for block B5 located downstream of the 11 to 14 October 2000 HPE event (Figure 7). This block formed on 13 October 0000 UTC. At this point in time approximately 38% of the trajectories ending in that block are strongly heated and of these more than 60% passed over an HPE area (Figure 11). These air masses experienced heating and ascent over the western North Atlantic (Figure 8b). The diabatic heating was most relevant for the initial phase of the block and remained at a lower level on 14 and 15 October 2000. On 16 October the fraction of strongly heated trajectories reached approximately 25% and the trajectories show that a part of these air masses experienced heating and ascent over North Africa and a part experienced heating and ascent along the Alpine southside in the HPE area related to the floods of Lago Maggiore on 14 October.

To test the reverse conclusion – i.e., that most air masses experiencing latent heating associated with HPEs contribute to the formation or maintenance of blocks - forward trajectories started from HPE areas are analysed. For the month under investigation we find a fraction of 21% (18%) and 8% (7%) of these strongly (moderately) heated air parcels to reach a weak and a strong block, respectively. A slightly higher fraction of the strongly heated air parcels reaches a block than the moderately heated parcels and more parcels reach weak blocks than strong blocks.

In summary, a substantial fraction of the air parcels in the block that experienced strong latent heating originated from HPE regions (>60%). Thus, the diabatic heating in the ascending air during HPEs could be of importance for the strength and the duration of blocks further down-

stream. Note however that only ~ 21% the air parcels in the HPE regions are steered into blocks in the 3 days after passing through the HPE region.

6. Discussion

Meridional amplification of the flow and the subsequent wave breaking and PV streamer formation are instrumental for HPEs on the Alpine south-side and blocks contribute to the flow amplification. Blocking upstream or downstream of a breaking wave (or both) can contribute to meridional amplification via strong deformation. An example flow configuration resulting in a strong deformation flow was present on 30 September with a positive PV anomaly in the north and a negative PV anomaly in the south upstream of the breaking wave and a negative PV anomaly in the north and positive PV anomaly in the south (a block; Figure 12). As summarized in the introduction the meridional amplification of the flow and the associated formation of PV streamers and cut-offs has been identified as flood conducive flow configuration in different locations around the world.

Blocking contributes to the stalling of the precipitation-conducive weather features, here a PV streamer, through modification of the background flow and hence the Rossby waveguide. An example is the HPE from 11 to 15 October 2000 (section 4.3). During this period, a PV streamer and later a high-PV cut-off remained quasi-stationary over western Europe for several days (Figure 7), moist air was continuously transported towards the Alpine south side (not shown, see Barton et al. 2016), and heavy precipitation fell. The stalling of this PV streamer was related to two blocks located downstream. During this time, a large block (B1) was located downstream over northern Russia (Figure 7). This block evolved from the Scandinavian blocking (B1) on 30 September (Figure 13). Even though this block was situated relatively far away from central Europe, the block over Russia affected the flow over Europe. Recurrent planetary-scale anticyclonic wave breaking along the eastern flank of the block (e.g., Figure 7a and b) interrupted the Rossby waveguide east of Europe. This is visible in the 10-days running mean of the 500 hPa zonal wind (Figure 13 and 14). The background zonal flow is either negative or weakly positive over central and eastern Europe. The slowing down

of the zonal wind in the region of the block started on 20 September and persisted until 15 October (Figure 13). This, together with a ridge that turned into a block (B5) over eastern Europe on 13 October, slowed down the eastward propagation of the PV streamer and cut-off over western Europe between 11 and 15 October (Figure 14).

The analysis of back trajectories started from the blocks revealed that about two-thirds of the air masses in the blocks underwent latent heating in HPE regions and associated PV depletion (section 5). Hence, the diabatic heating associated with HPEs can contribute to the formation of a new downstream block or re-enforce an existing downstream block. In a sense the heavy precipitation and the block are both "side products" of the latent heat release. This block in turn, might through one of the processes described above, foster the formation of a next HPE upstream of the block. For example, B1 on 22 September was partly fed by air experiencing latent heating during the first HPE on 20 September over the Lago Maggiore catchment (see Section 4.1 and Figure 4c, d). B1 was later also involved in the formation of the second and third HPE. However, B1 was very large and long living and the isolated effect of the first HPE on 20 September on the lifecycle of B1 was probably small.

Ascending air masses, strong latent heat release and associated upper-level PV depletion are characteristics of WCBs (Madonna et al. 2014, Schemm et al. 2013) and heavy precipitation is often related to WCBs (Pfahl et al.2014). Hence as pointed out in the detailed case descriptions some of the strongly heated air masses coincide with WCBs and hence WCB outflow contributes to blocking (see also Schneidereit et al. 2017). However, the definition of strongly heated trajectories use here is broader than the WCB definition and includes other air masses. It would be interesting in a future study to specifically quantify the WCB contributions to blocks.

5 Conclusions

We study dynamical links between heavy precipitation events (HPEs), a flood and atmospheric blocking based on the case of a large flood event in October 2000 in the Lago Maggiore in southern Switzerland. Within one month between 15 September 2000 and 15 October 2000, a series of three HPEs that exceeded the local 95th seasonal percentile of daily accumulations unfolded. All three HPEs contributed to the rise of the lake level, and the strongest rise occurred during the long-lasting third HPE, when it crossed the flood threshold.

Blocks contributed to the flood event both via dry and moist dynamics and the following dynamical links were found:

- First, blocks were associated with recurring HPEs at the same location. Upstream of a block over Scandinavia a very similar flow pattern with a PV streamer located to the west of Switzerland occurred twice at the same location within 10 days and resulted both times in heavy precipitation. The flow field upstream of the Scandinavian block contributed to the formation and meridional elongation of these PV streamers.
- Second, the stalling of the eastward propagation of a PV streamer (and later a high-PV cut-off) upstream of a blocked area lead to a prolonged period of heavy precipitation over the same region. The stalling was related i) to a direct blocking of the eastward progression of the cut-off by a downstream block over eastern Europe and ii) long lasting blocks further downstream that interrupted the waveguide by reducing the zonal background flow to almost zero downstream of Switzerland.
- In terms of moist dynamics upper-level PV depletion by latent heat release is important for blocking dynamics (Pfahl et al. 2016). In our case study month 39% of the air masses in the blocks experienced diabatic heating of more than 2K during their transport to the upper troposphere within three days prior to arriving in the block. The fraction of strongly (>5K) diabatically heated air masses is 27%. The almost two

thirds (63%) of these strongly diabatically influenced air masses reached the blocks from regions of heavy precipitation (>95th seasonal percentile).

6 Acknowledgements

We would like to thank Marco Rohrer for implementation of the block detection algorithm, Yannick Barton for the supply of the precipitation data from the Lago Maggiore catchment and Erica Madonna for the WCB outflow data. Furthermore, we would like to thank the two anonymous reviewers for their helpful comments that contributed to substantially improve the quality of this study. This research was funded by the Swiss National Science Foundation, Project No. 156059.

7 References

Altenhoff, A. M., O. Martius, M. Croci-maspoli, C. Schwierz, and H. C. Davies, 2008: Linkage of atmospheric blocks and synoptic-scale Rossby waves: A climatological analysis. *Tellus, Ser. A Dyn. Meteorol. Oceanogr.*, **60**, 1053–1063, doi:10.1111/j.1600-0870.2008.00354.x.

Antokhina, O. Y., P. N. Antokhin, E. V. Devyatova, and Y. V. Martynova, 2018: Atmospheric Blockings in Western Siberia. Part 2. Long-term Variations in Blocking Frequency and Their Relation with Climatic Variability over Asia. *Russ. Meteorol. Hydrol.*, **43**, 143–151, doi:10.3103/s1068373918030020.

Barton, Y., P. Giannakaki, H. von Waldow, C. Chevalier, S. Pfahl, and O. Martius, 2016: Clustering of Regional-Scale Extreme Precipitation Events in Southern Switzerland. *Mon. Weather Rev.*, **144**, 347–369, doi:10.1175/MWR-D-15-0205.1.

Bieli, M., S. Pfahl, and H. Wernli, 2015: A lagrangian investigation of hot and cold temperature extremes in europe. *Q. J. R. Meteorol. Soc.*, **141**, 98–108, doi:10.1002/qj.2339.

BWG, 2002: Hochwasser 2000 - Les crues 2000. *Berichte des BWG, Serie Wasser*, doi:PNR61.

Carrera, M. L., R. W. Higgins, and V. E. Kousky, 2004: Downstream weather impacts associated with atmospheric blocking over the Northeast Pacific. *J. Clim.*, **17**, 4823–4839, doi:10.1175/JCLI-3237.1.

Croci-Maspoli, M., and H. C. Davies, 2009: Key Dynamical Features of the 2005/06 European Winter. *Mon. Weather Rev.*, **137**, 664–678, doi:10.1175/2008MWR2533.1.

Dee, D. P., and Coauthors, 2011: The ERA-Interim reanalysis: Configuration and performance of the data assimilation system. *Q. J. R. Meteorol. Soc.*, **137**, 553–597, doi:10.1002/qj.828.

Dole, R., and Coauthors, 2011: Was there a basis for anticipating the 2010 Russian heat wave? *Geophys. Res. Lett.*, **38**, doi:10.1029/2010GL046582.

Fehlmann, R., C. Quadri, and H. Davies, 2000: An Alpine rainstorm: Sensitivity to the mesoscale upper-level structure. *Weather Forecast.*, **15**, 4–28, doi:10.1175/1520-0434(2000)015<0004:AARSTT>2.0.CO;2.

Fernandes, L. G., and R. R. Rodrigues, 2017: Changes in the patterns of extreme rainfall events in southern Brazil. *Int. J. Climatol.*, doi:10.1002/joc.5248.

Frei, C., and C. Schär, 1998: A precipitation climatology of the Alps from high-resolution rain-gauge observations. *Int. J. Climatol.*, **18**, 873–900, doi:10.1002/(SICI)1097-0088(19980630)18:8<873::AID-JOC255>3.0.CO;2-9.

Froidevaux, P., and O. Martius, 2016: Exceptional integrated vapour transport toward orography: an important precursor to severe floods in Switzerland. *Q. J. R. Meteorol. Soc.*, **142**, 1997–2012, doi:10.1002/qj.2793.

Grams, C. M., H. Binder, S. Pfahl, N. Piaget, and H. Wernli, 2014: Atmospheric processes triggering the central European floods in June 2013. *Nat. Hazards Earth Syst. Sci.*, **14**, 1691–1702, doi:10.5194/nhess-14-1691-2014.

Haylock, M., H. N, K. T. AMG, K. EJ, J. PD, and N. M., 2008: A European daily higher-solution gridded data set of surface temperature and precipitation for 1950-2006. *J Geophys Res*, **113**.

Hong, C., H.-H. Hsu, N.-H. Lin, and H. Chiu, 2011: Roles of European blocking and tropical-extratropical interaction in the 2010 Pakistan flooding. *Geophys. Res. ...*, **38**.

Jacobeit, J., A. Philipp, and M. Nonnenmacher, 2006: Atmospheric circulation dynamics linked with prominent discharge events in Central Europe. *Hydrol. Sci. J.*, **51**, 946–965, doi:10.1623/hysj.51.5.946.

Kelman, I., 2001: The autumn 2000 floods in England and flood management. *Weather*, **56**, 346–360, doi:10.1002/j.1477-8696.2001.tb06507.x.

Krishnamurti, T. N., T. S. V. Vijaya Kumar, K. Rajendran, and A. Hopkins, 2003: Antecedents of the flooding over southeastern England during October 2000. *Weather*, **58**, 367–370, doi:10.1256/wea.230.02.

Lackmann, G. M., D. Keyser, and L. F. Bosart, 1997: A Characteristic Life Cycle of Upper-Tropospheric Cyclogenetic Precursors during the Experiment on Rapidly Intensifying Cyclones over the Atlantic (ERICA). *Mon. Weather Rev.*, **125**, 2729–2758.

Lau, W. K. M., and K.-M. Kim, 2012: The 2010 Pakistan Flood and Russian Heat Wave: Teleconnection of Hydrometeorological Extremes. *J. Hydrometeorol.*, **13**, 392–403, doi:10.1175/JHM-D-11-016.1.

Madonna, E., H. Wernli, H. Joos, and O. Martius, 2014: Warm conveyor belts in the ERA-Interim Dataset (1979-2010). Part I: Climatology and potential vorticity evolution. *J. Clim.*, **27**, 3–26, doi:10.1175/JCLI-D-12-00720.1.

Marsh, T. J., 2001: The 2000/01 floods in the UK - a brief overview. *Weather*, **56**, 343–345, doi:10.1002/j.1477-8696.2001.tb06506.x.

Martius, O., E. Zenklusen, C. Schwierz, and H. C. Davies, 2006: Episodes of Alpine heavy precipitation with an overlying elongated stratospheric intrusion: A climatology. *Int. J. Climatol.*, **26**, 1149–1164, doi:10.1002/joc.1295.

Martius, O., and Coauthors, 2013: The role of upper-level dynamics and surface processes for the Pakistan flood of July 2010. *Q. J. R. Meteorol. Soc.*, **139**, 1780–1797, doi:10.1002/qj.2082.

Massacand, A. C., H. Wernli, and H. C. Davies, 1998: Heavy precipitation on the alpine southside: An upper-level precursor. *Geophys. Res. Lett.*, **25**, 1438, doi:10.1029/98GL50869.

Massacand, A. C., H. Wernli, H. C. Davies, A. C. Massacand, H. Wernli, and H. C. Davies, 2001: Influence of Upstream Diabatic Heating upon an Alpine Event of Heavy Precipitation. *Mon. Weather Rev.*, **129**, 2822–2828, doi:10.1175/1520-

0493(2001)129<2822:IOUDHU>2.0.CO;2.

MeteoSwiss, 2016: *Daily Precipitation (final analysis): RhiresD. Documentation of MeteoSwiss Grid-Data Products*. 4 pp.

Milrad, S. M., J. R. Gyakum, and E. H. Atallah, 2015: A Meteorological Analysis of the 2013 Alberta Flood: Antecedent Large-Scale Flow Pattern and Synoptic–Dynamic Characteristics. *Mon. Weather Rev.*, **143**, 2817–2841, doi:10.1175/MWR-D-14-00236.1.

Pelly, J. L., and B. J. Hoskins, 2003: A New Perspective on Blocking. *J. Atmos. Sci.*, **60**, 743–755, doi:10.1175/1520-0469(2003)060<0743:ANPOB>2.0.CO;2.

Pfahl, S., and H. Wernli, 2012a: Quantifying the relevance of atmospheric blocking for co-located temperature extremes in the Northern Hemisphere on (sub-)daily time scales. *Geophys. Res. Lett.*, **39**, n/a-n/a, doi:10.1029/2012GL052261.

Pfahl, S., and H. Wernli, 2012b: Quantifying the Relevance of Cyclones for Precipitation Extremes. *J. Clim.*, **25**, 6770–6780, doi:10.1175/JCLI-D-11-00705.1.

——, E. Madonna, M. Boettcher, H. Joos, and H. Wernli, 2014: Warm conveyor belts in the ERA-Interim data set (1979-2010). Part II: Moisture origin and relevance for precipitation. *J. Clim.*, 130822114529004, doi:10.1175/JCLI-D-13-00223.1.

Pfahl, S., C. Schwierz, M. Croci-Maspoli, C. M. Grams, and H. Wernli, 2015: Importance of latent heat release in ascending air streams for atmospheric blocking. *Nat. Geosci.*, **8**, 610–614, doi:10.1038/ngeo2487.

Piaget, N., P. Froidevaux, P. Giannakaki, F. Gierth, O. Martius, M. Riemer, G. Wolf, and C. M. Grams, 2015: Dynamics of a local Alpine flooding event in October 2011: Moisture source and large-scale circulation. *Q. J. R. Meteorol. Soc.*, **141**, 1922–1937, doi:10.1002/qj.2496.

Rex, D. F., 1950: Blocking Action in the Middle Troposphere and its Effect upon Regional Climate: II. The Climatology of Blocking Action. *Tellus*, **2**, 196–211, doi:10.1111/j.2153-3490.1950.tb00331.x.

Rex, D. F., 1951: The Effect of Atlantic Blocking Action upon European Climate. *Tellus*, **3**, 100–112, doi:10.1111/j.2153-3490.1951.tb00784.x.

Rodrigues, R. R., T. Woollings, R. R. Rodrigues, and T. Woollings, 2017: Impact of Atmospheric Blocking on South America in Austral Summer. *J. Clim.*, **30**, 1821–1837, doi:10.1175/JCLI-D-16-0493.1.

Samel, A. N., and X. Z. Liang, 2003: Understanding relationships between the 1998 Yangtze River flood and northeast Eurasian blocking. *Clim. Res.*, **23**, 149–158, doi:10.3354/cr023149.

Saunders, F., M. Göber, and B. Chalcraft, 2001: The exceptional rainfall event of 11 and 12 October 2000 in Kent and Sussex, as observed and as forecast by the Met Office Mesoscale Model. *Weather*, **56**, 360–367, doi:10.1002/j.1477-8696.2001.tb06508.x.

Schneidereit, A., D.H. Peters, C.M. Grams, J.F. Quinting, J.H. Keller, G. Wolf, F. Teubler, M. Riemer, and O. Martius, 2017: Enhanced Tropospheric Wave Forcing of Two Anticyclones in the Prephase of the January 2009 Major Stratospheric Sudden Warming Event. *Mon. Wea. Rev.*, **145**, 1797–1815, https://doi.org/10.1175/MWR-D-16-0242.1

Schemm, S., Wernli, H., & Papritz, L. (2013). Warm Conveyor Belts in Idealized Moist Baroclinic Wave Simulations*. Journal of the Atmospheric Sciences, 70(2), 627–652. https://doi.org/10.1175/JAS-D-12-0147.1

Schwierz, C., M. Croci-Maspoli, and H. C. Davies, 2004: Perspicacious indicators of atmospheric blocking. *Geophys. Res. Lett.*, **31**, L06125, doi:10.1029/2003GL019341.

Shutts, G. J., 1983: The propagation of eddies in diffluent jetstreams: Eddy vorticity forcing of 'blocking' flow fields. *Q. J. R. Meteorol. Soc.*, **109**, 737–761, doi:10.1002/qj.49710946204.

Sillmann, J., and M. Croci-Maspoli, 2009: Present and future atmospheric blocking and its impact on European mean and extreme climate. *Geophys. Res. Lett.*, **36**, doi:10.1029/2009GL038259.

Small, D., E. Atallah, and J. R. Gyakum, 2014: An objectively determined blocking index and its Northern Hemisphere climatology. *J. Clim.*, **27**, 2948–2970, doi:10.1175/JCLI-D-13-00374.1.

Sousa, P. M., D. Barriopedro, R. M. Trigo, A. M. Ramos, R. Nieto, L. Gimeno, K. F. Turkman, and M. L. R. Liberato, 2016: Impact of Euro-Atlantic blocking patterns in iberia precipitation using a novel high resolution dataset. *Clim. Dyn.*, **46**, 2573–2591, doi:10.1007/s00382-015-2718-7.

——, R. M. Trigo, D. Barriopedro, P. M. M. Soares, A. M. Ramos, and M. L. R. Liberato, 2017: Responses of European precipitation distributions and regimes to different blocking locations. *Clim. Dyn.*, **48**, 1141–1160, doi:10.1007/s00382-016-3132-5.

Sprenger, M., and H. Wernli, 2015: The LAGRANTO Lagrangian analysis tool -- version 2.0. *Geosci. Model Dev.*, **8**, 2569–2586, doi:10.5194/gmd-8-2569-2015.

Stucki, P., R. Rickli, S. Brönnimann, O. Martius, H. Wanner, D. Grebner, and J. Luterbacher, 2012: Weather patterns and hydro-climatological precursors of extreme floods in Switzerland since 1868. *Meteorol. Zeitschrift*, **21**, 531–550, doi:10.1127/0941-2948/2012/368.

Trigo, R. M., I. F. Trigo, C. C. DaCamara, and T. J. Osborn, 2004: Climate impact of the European winter blocking episodes from the NCEP/NCAR reanalyses. *Clim. Dyn.*, **23**, 17–28, doi:10.1007/s00382-004-0410-4.

Wernli, H., and H. C. Davies, 1997: A Lagrangian-based analysis of extratropical cyclones .1. The method and some applications. *Q. J. R. Meteorol. Soc.*, **123**, 467–489, doi:10.1256/smsqj.53810.

Whan, K., F. Zwiers, and J. Sillmann, 2016: The influence of atmospheric blocking on extreme winter minimum temperatures in North America. *J. Clim.*, **29**, 4361–4381, doi:10.1175/JCLI-D-15-0493.1.

Yamada, T. J., D. Takeuchi, M. A. Farukh, and Y. Kitano, 2016: Climatological

Characteristics of Heavy Rainfall in Northern Pakistan and Atmospheric Blocking over Western Russia. *J. Clim.*, **29**, 7743–7754, doi:10.1175/JCLI-D-15-0445.1.

Yao, Y., and D. H. Luo, 2014: The Anomalous European Climates Linked to Different Euro-Atlantic Blocking. *Atmos. Ocean. Sci. Lett.*, **7**, 309–313, doi:10.3878/j.issn.1674-2834.14.0001.

Figure Captions

Figure 1: Accumulated precipitation [colour shading, mm] over Europe between 15 September 2000 and 15 October 2000, the month prior to the great floods of south-east England and of the Lago Maggiore as recorded in (a) the E-OBS data and (b) the ERA-Interim data. The hatched areas show the regions where the local 95th percentile of the monthly precipitation in the same time of the year was exceeded. The circle indicates the Location of the Lago Maggiore.

Figure 2: (a) Daily precipitation sums for the Lago Maggiore catchment: with 95th percentile (dashed) precipitation threshold. The blue shaded area indicates the mean daily water level of Lago Maggiore measured at Locarno. The red line indicates the 195.75 m a.s.l. flood threshold of Lago Maggiore, the blue solid line indicates the all-year climatological (1961-2012) mean lake level and the blue dashed lines show the mean plus and minus one standard deviation of the daily values (adapted from Figure 5 in Barton et al. 2015). (b) Location of the Lago Maggiore (blue) relative to Switzerland (yellow) and the topography (shadings).

Figure 3: Evolution of PV on 325K (shaded) in ERA-Interim on 16, 17 and 18 September 0000 UTC (a-c), from 19 September 1800 UTC to 20 September 1800 UTC in 12h steps (d-h), on 21 September 0000 UTC and on 22 September 1800 UTC. The green lines indicate blockings after Schwierz et al. (2004) with PV thresholds of -1.3pvu (dark green) and -1.0pvu (light green) respectively. The purple areas indicate regions in which the daily precipitation accumulations exceed the 95th percentile with respect to the autumn (SON) climatology from 1979-2015 and the arrows indicate the (>20m/s) wind on 325K.

Figure 4: Left: Mean sea level pressure [hPa] (black contours), dynamical tropopause (2 pvu) on 325K in red, strong blockings after Schwierz et al. (2004) in dark green on (a) 18 September 2000, 1800 UTC and (c) 20 September 2000, 1800 UTC. The purple areas indicate re-

gions in which the daily precipitation accumulations exceed the 95th percentile with respect to the autumn (SON) climatology from 1979-2015. Right: strongly diabatically heated (>5K) backwards trajectories (-72h), that passed through a HPE region and that were at the same time almost saturated (>80%RH), started in the region of strong blocks on (b) 20 September, 18 UTC and on (d) 22 September, 18 UTC. Colors indicate the pressure [hPa] and the black dots indicate the position of the air parcels at t=0 and t=-48h.

Figure 5: Same as Figure 3 in steps from 24 September 2000, 00UTC to 30 September 2000, 00UTC in 24h time steps.

Figure 6: Same as Figure 4 on (a) 22 September 2000, 12UTC and on (b) 24 September 2000, 12UTC.

Figure 7: Same as Figure 3 but on 07 October 2000, 12 UTC and from 11 October 2000, 12 UTC to 16 October 2000, 12 UTC in 12h time steps.

Figure 8: Same as Figure 4 on (a) 11 October 2000, 12 UTC, (b) 12 October 2000, 06 UTC and (c) 13 October 2000, 12 UTC and (d)14 October 2000, 06 UTC.

Figure 9: Left: Monthly fraction of air masses in the block that were moderately (>2K) and strongly (>5K) diabatically heated within the 72h hours before in dark gray and the fraction that additionally passed through a heavy precipitation region (>95th percentile) while being quasi-saturated (RH>80%) in light gray. Right: Monthly fraction of quasi-saturated air masses in the precipitation regions that were moderately (>2K) and strongly (>5K) diabatically heated within the 72h after in dark gray and the fraction that additionally passed through a weak block in light gray.

Figure 10: Daily fraction of strongly diabatically heated air masses in the strong blocks that passed through a region of heavy precipitation (>95th percentile) within the 72h before while being quasi-saturated (RH>80%) from 15 September 2000 to 15 October 2000. The red line

indicates the median over all time steps and the gray lines show range of +- 1 standard deviations.

Figure 11: (a) Fraction of moderately (>2K, orange) and strongly (>5K, darkred) heated trajectories with respect to all trajectories in block B5 from 11 to 22 October 2000 and the fraction of strongly diabatically heated trajectories that derive from HPE regions (blue). The gray shading indicates the relative size of the block in %. (b) 72h backward trajectories from 16 October, 1800 UTC to 13 October, 1800 UTC. The colors indicate pressure [hPa] and the black crosses indicate the location at t=0 and t=-48h.

Figure 12: Vertically averaged (500hPa-150hPa) potential vorticity anomalies on 30 September, 00UTC with reference to the average 30-day running mean at the same date between 1979-2015.

Figure 13: Evolution of meridionally averaged (30-80°N) low frequency (10-days running mean) zonal wind in 500hPa from 20 September 2000 to 15 October 2000. The darkgreen (green) dashed regions indicate the presence of a strong (weak) block between 30°N and 80°N.

Figure 14: 10-days running mean of the zonal wind on 500hPa on 12 October 2000, 1200 UTC (a) and 14 October 2000 1200 UTC (b) (shading) and the position of the dynamical tropopause at 325K (contours) on 24h before (yellow), 12h before (orange), at the time (red) and 12h later (purple) and 24h later (pink). The green (darkgreen) indicates the location of the weak (strong) blocks.

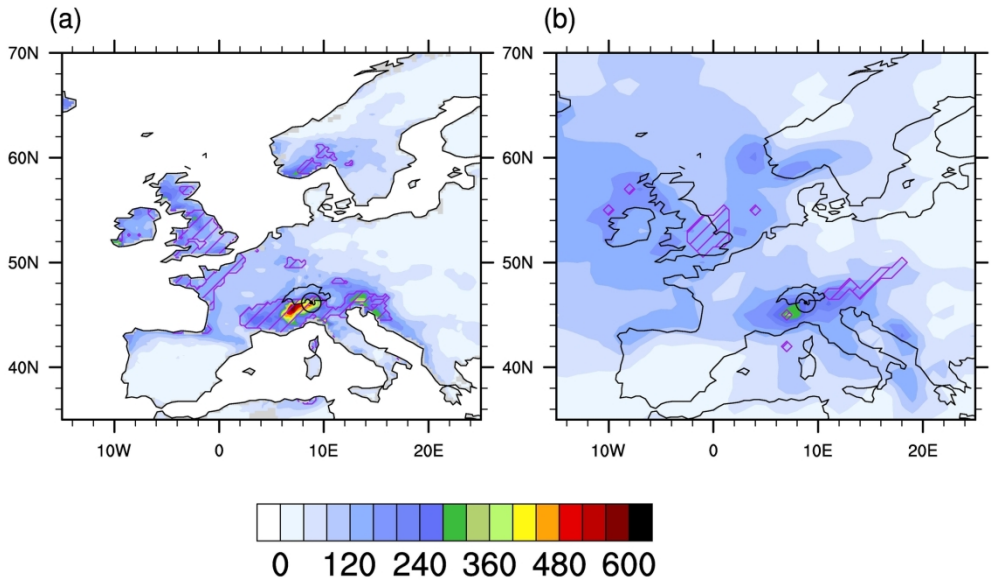

Figure 1. Accumulated precipitation [colour shading, mm] over Europe between 15 September 2000 and 15 October 2000, the month prior to the great floods of south-east England and of the Lago Maggiore as recorded in (a) the E-OBS data and (b) the ERA-Interim data. The hatched areas show the regions where the local 95th percentile of the monthly precipitation in the same time of the year was exceeded. The circle indicates the Location of the Lago Maggiore.

183x107mm (300 x 300 DPI)

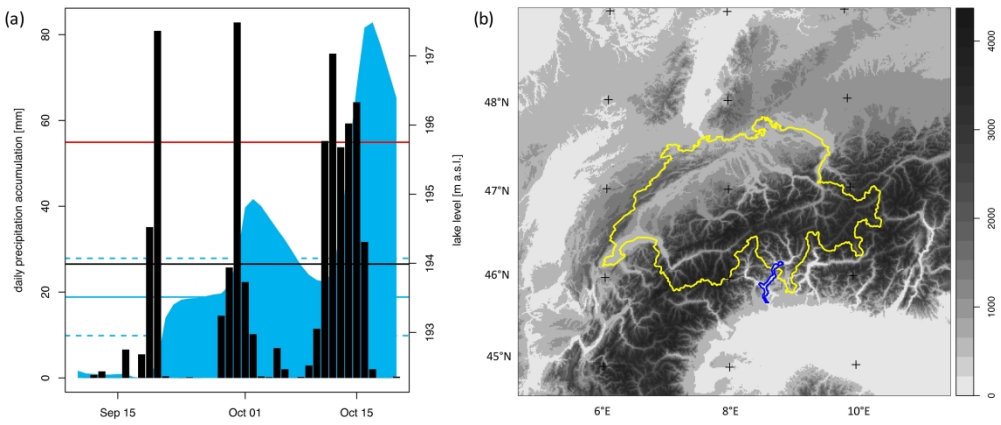

Figure 2. (a) Daily precipitation sums for the Lago Maggiore catchment: with 95th percentile (dashed) precipitation threshold. The blue shaded area indicates the mean daily water level of Lago Maggiore measured at Locarno. The red line indicates the 195.75 m a.s.l. flood threshold of Lago Maggiore, the blue solid line indicates the all-year climatological (1961-2012) mean lake level and the blue dashed lines show the mean plus and minus one standard deviation of the daily values (adapted from Figure 5 in Barton et al. 2015). (b) Location of the Lago Maggiore (blue) relative to Switzerland (yellow) and the topography (shadings).

337x142mm (300 x 300 DPI)

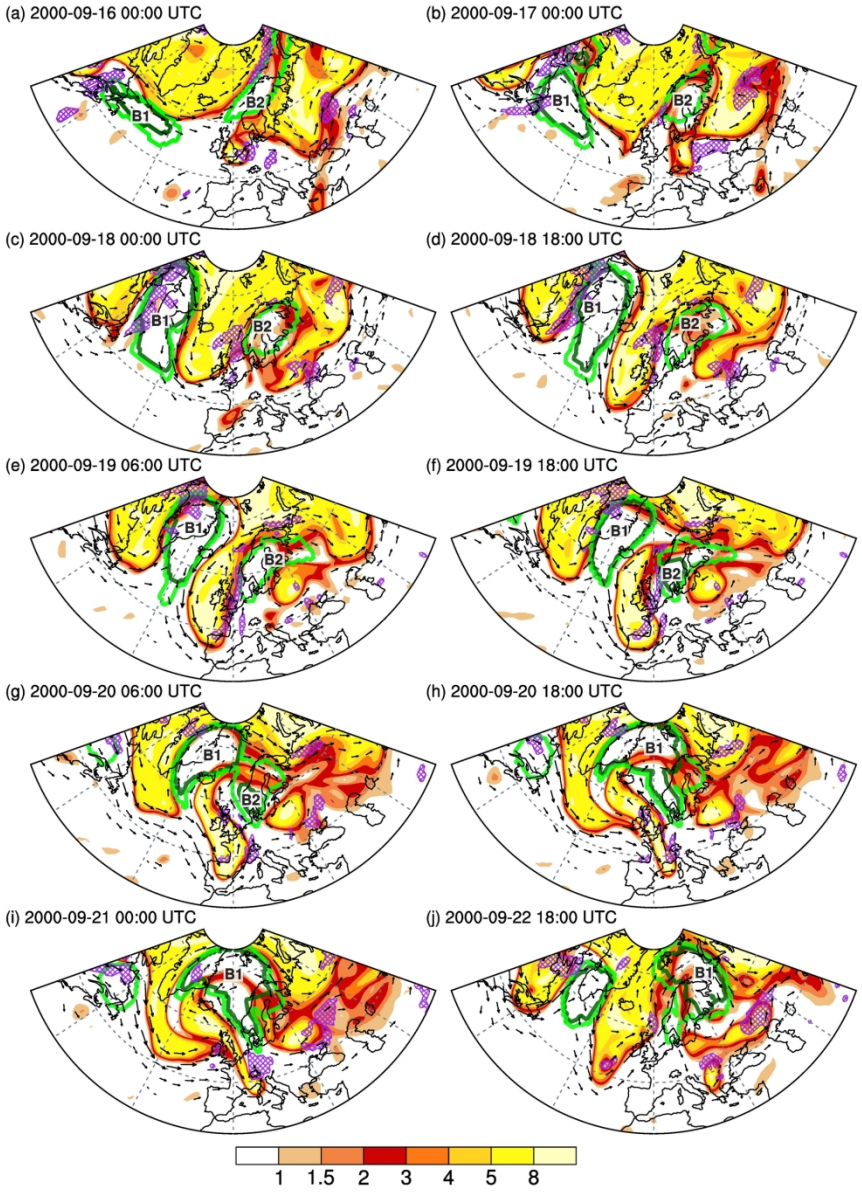

Figure 3. Evolution of PV on 325K (shaded) in ERA-Interim on 16, 17 and 18 September 0000 UTC (a-c), from 19 September 1800 UTC to 20 September 1800 UTC in 12h steps (d-h), on 21 September 0000 UTC and on 22 September 1800 UTC. The green lines indicate blockings after Schwierz et al. (2004) with PV thresholds of -1.3pvu (dark green) and -1.0pvu (light green) respectively. The purple areas indicate regions in which the daily precipitation accumulations exceed the 95th percentile with respect to the autumn (SON) climatology from 1979-2015 and the arrows indicate the (>20m/s) wind on 325K.

161x221mm (300 x 300 DPI)

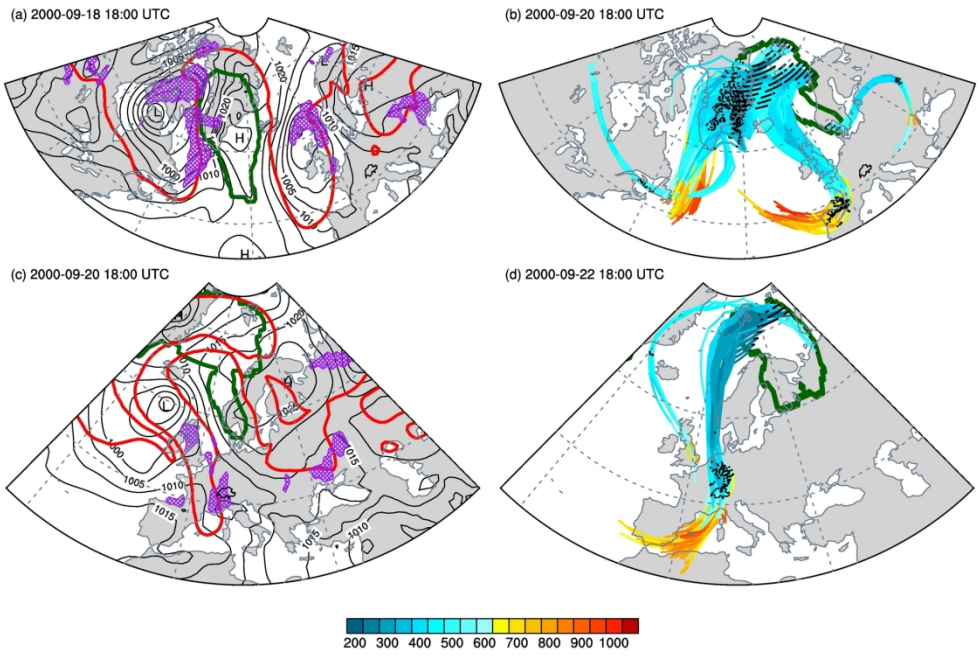

Figure 4. Left: Mean sea level pressure [hPa] (black contours), dynamical tropopause (2 pvu) on 325K in red, strong blockings after Schwierz et al. (2004) in dark green on (a) 18 September 2000, 1800 UTC and (c) 20 September 2000, 1800 UTC. The purple areas indicate regions in which the daily precipitation accumulations exceed the 95th percentile with respect to the autumn (SON) climatology from 1979-2015. Right: strongly diabatically heated (>5K) backwards trajectories (-72h), that passed through a HPE region and that were at the same time almost saturated (>80%RH), started in the region of strong blocks on (b) 20 September, 18 UTC and on (d) 22 September, 18 UTC. Colors indicate the pressure [hPa] and the black dots indicate the position of the air parcels at t=0 and t=-48h.

184x121mm (300 x 300 DPI)

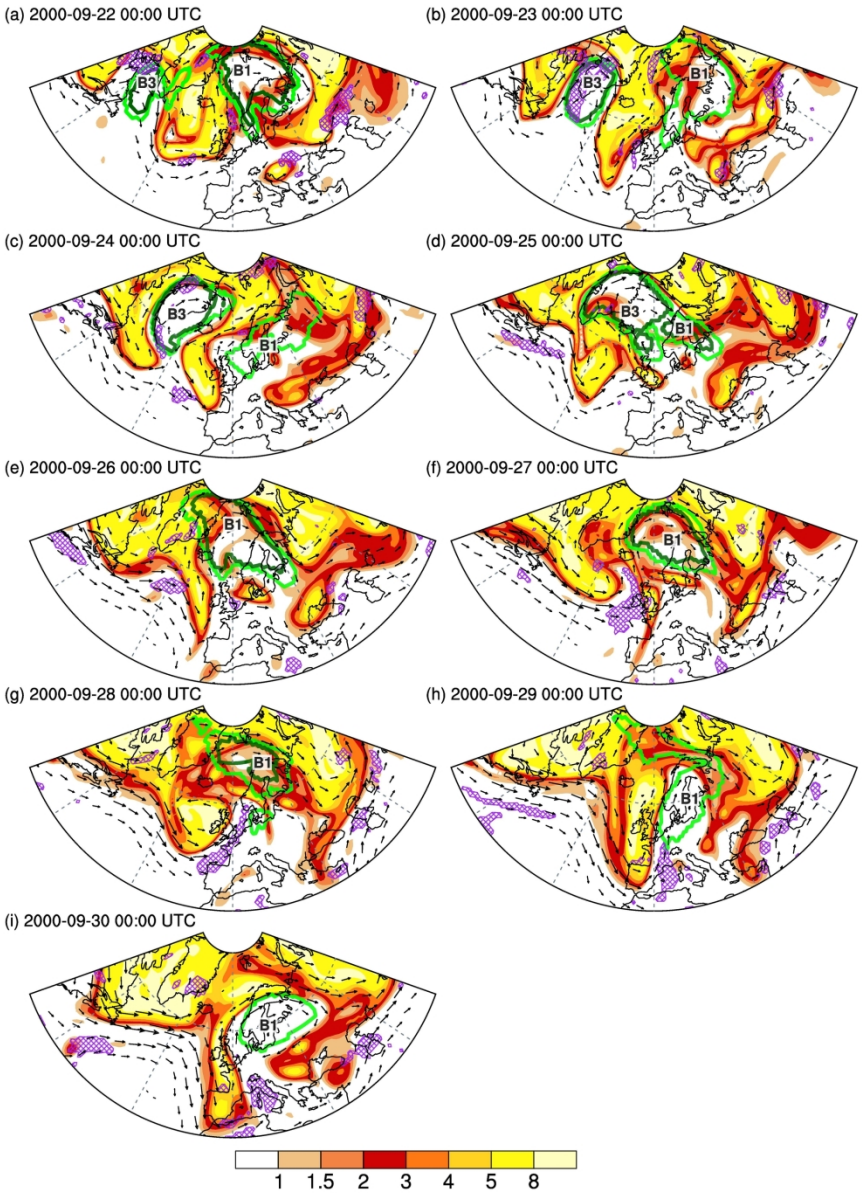

Figure 5. Same as Figure 3 in steps from 24 September 2000, 00UTC to 30 September 2000, 00UTC in 24h time steps.

178x244mm (300 x 300 DPI)

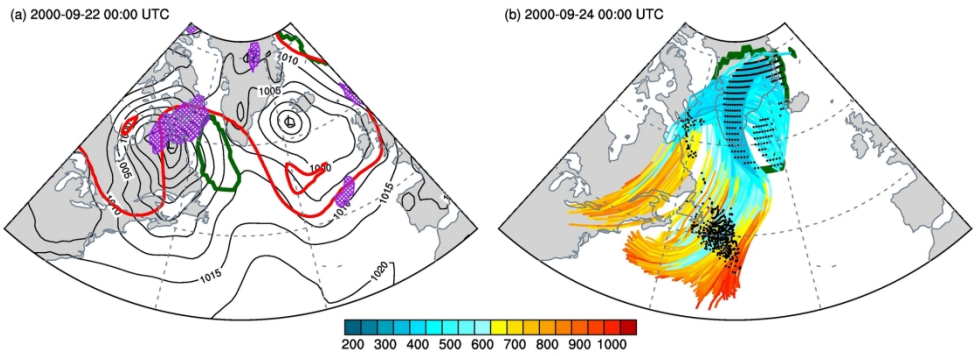

Figure 6. Same as Figure 4 on (a) 22 September 2000, 12UTC and on (b) 24 September 2000, 12UTC.

184x66mm (300 x 300 DPI)

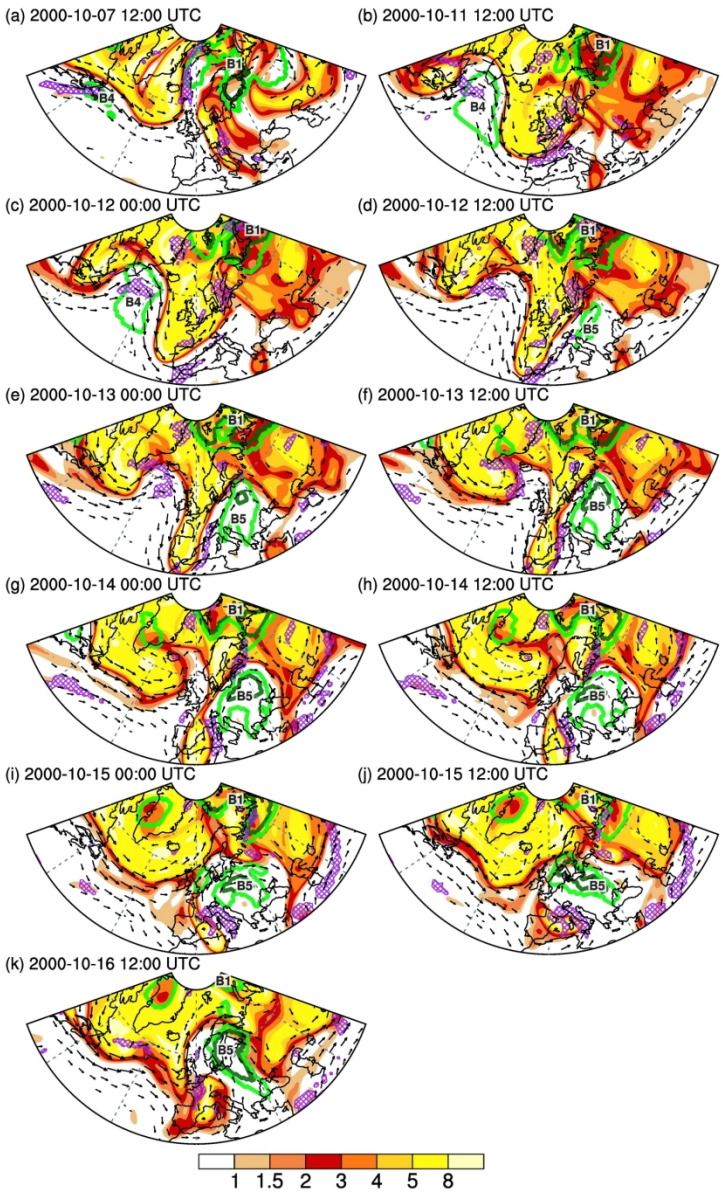

Figure 7. Same as Figure 3 but on 07 October 2000, 12 UTC and from 11 October 2000, 12 UTC to 16 October 2000, 12 UTC in 12h time steps.

136x221mm (300 x 300 DPI)

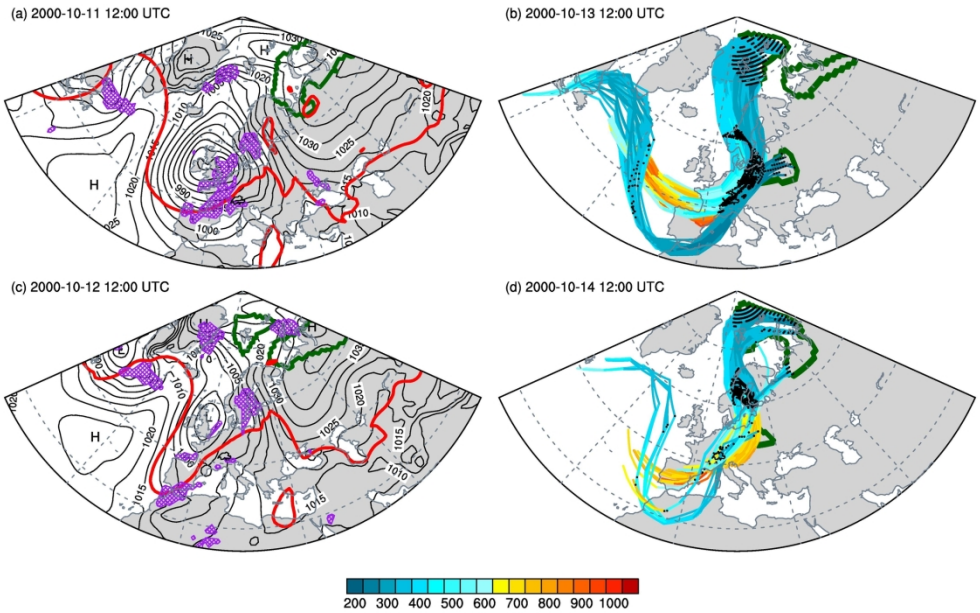

Figure 8. Same as Figure 4 on (a) 11 October 2000, 12 UTC, (b) 12 October 2000, 06 UTC and (c) 13 October 2000, 12 UTC and (d)14 October 2000, 06 UTC.

184x114mm (300 x 300 DPI)

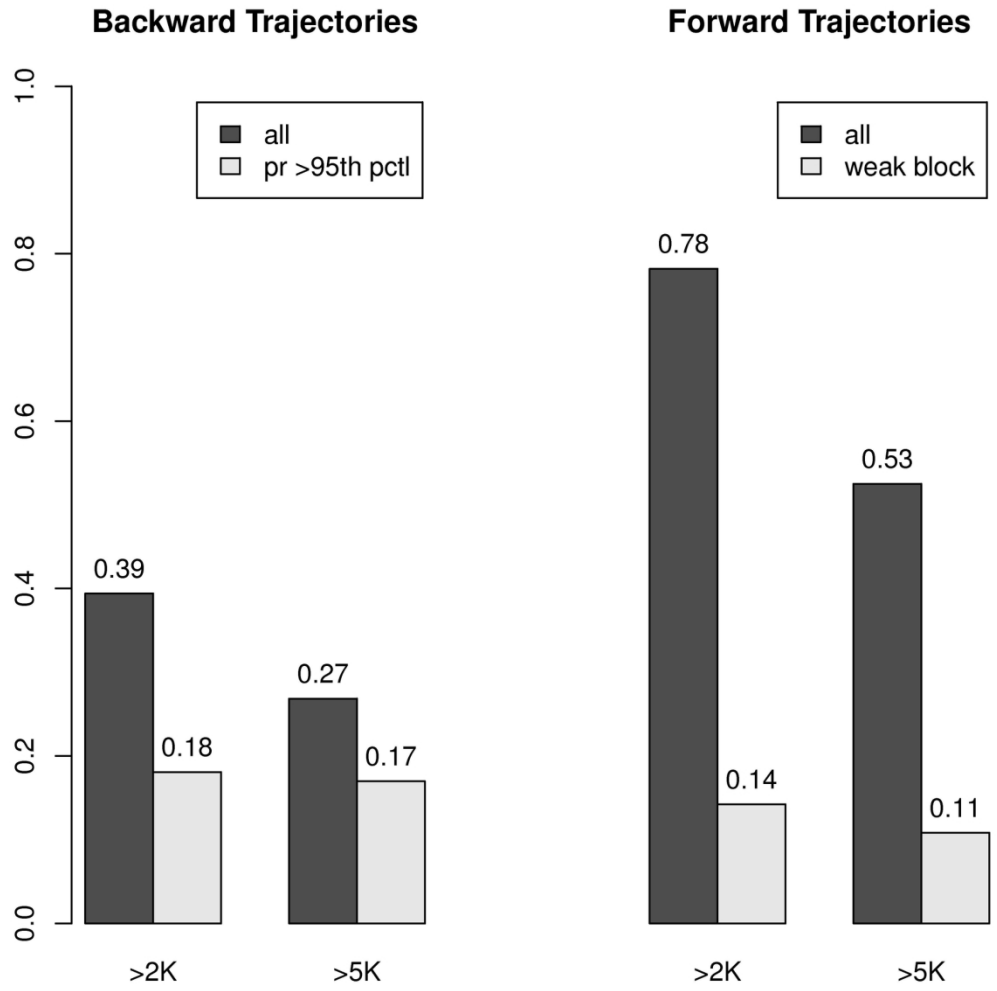

Figure 9. Left: Monthly fraction of air masses in the block that were moderately (>2K) and strongly (>5K) diabatically heated within the 72h hours before in dark gray and the fraction that additionally passed through a heavy precipitation region (>95th percentile) while being quasi-saturated (RH>80%) in light gray. Right: Monthly fraction of quasi-saturated air masses in the precipitation regions that were moderately (>2K) and strongly (>5K) diabatically heated within the 72h after in dark gray and the fraction that additionally passed through a weak block in light gray.

159x158mm (300 x 300 DPI)

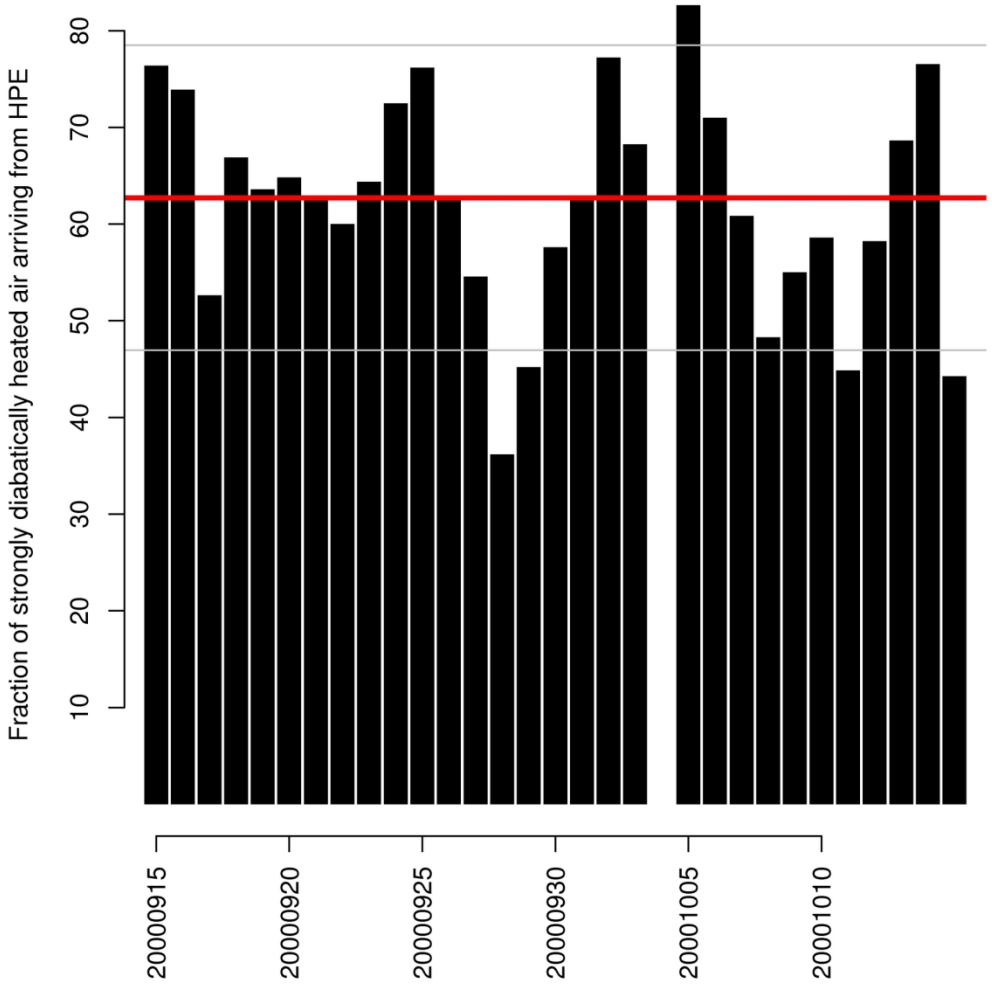

Figure 10. Daily fraction of strongly diabatically heated air masses in the strong blocks that passed through a region of heavy precipitation (>95th percentile) within the 72h before while being quasi-saturated (RH>80%) from 15 September 2000 to 15 October 2000. The red line indicates the median over all time steps and the gray lines show range of +- 1 standard deviations.

167x166mm (300 x 300 DPI)

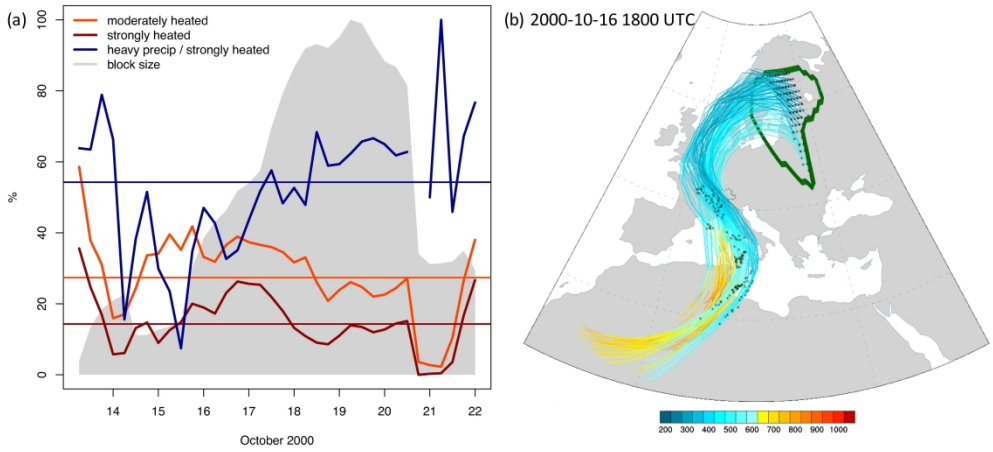

Figure 11. (a) Fraction of moderately (>2K, orange) and strongly (>5K, darkred) heated trajectories with respect to all trajectories in block B5 from 11 to 22 October 2000 and the fraction of strongly diabatically heated trajectories that derive from HPE regions (blue). The gray shading indicates the relative size of the block in %. (b) 72h backward trajectories from 16 October, 1800 UTC to 13 October, 1800 UTC. The colors indicate pressure [hPa] and the black crosses indicate the location at t=0 and t=-48h.

339x155mm (300 x 300 DPI)

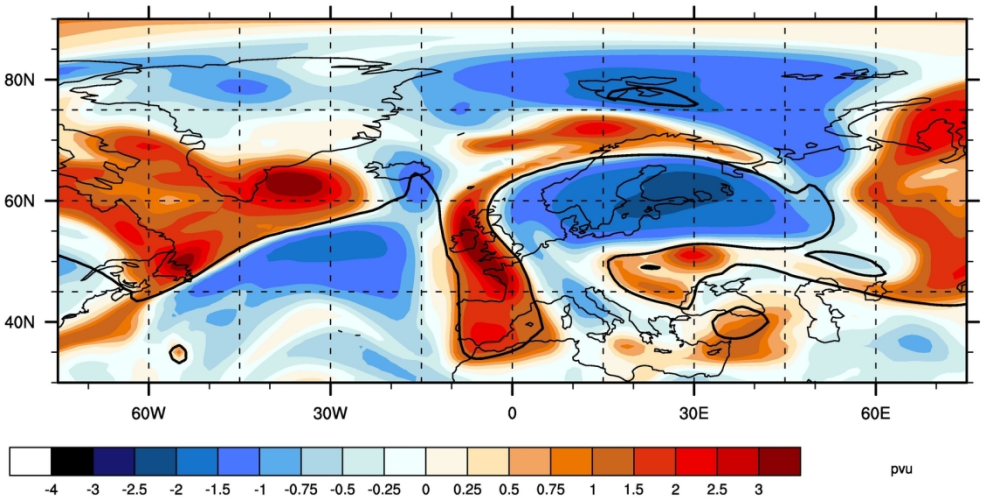

Figure 12. Vertically averaged (500hPa-150hPa) potential vorticity anomalies on 30 September, 00UTC with reference to the average 30-day running mean at the same date between 1979-2015.

155x80mm (300 x 300 DPI)

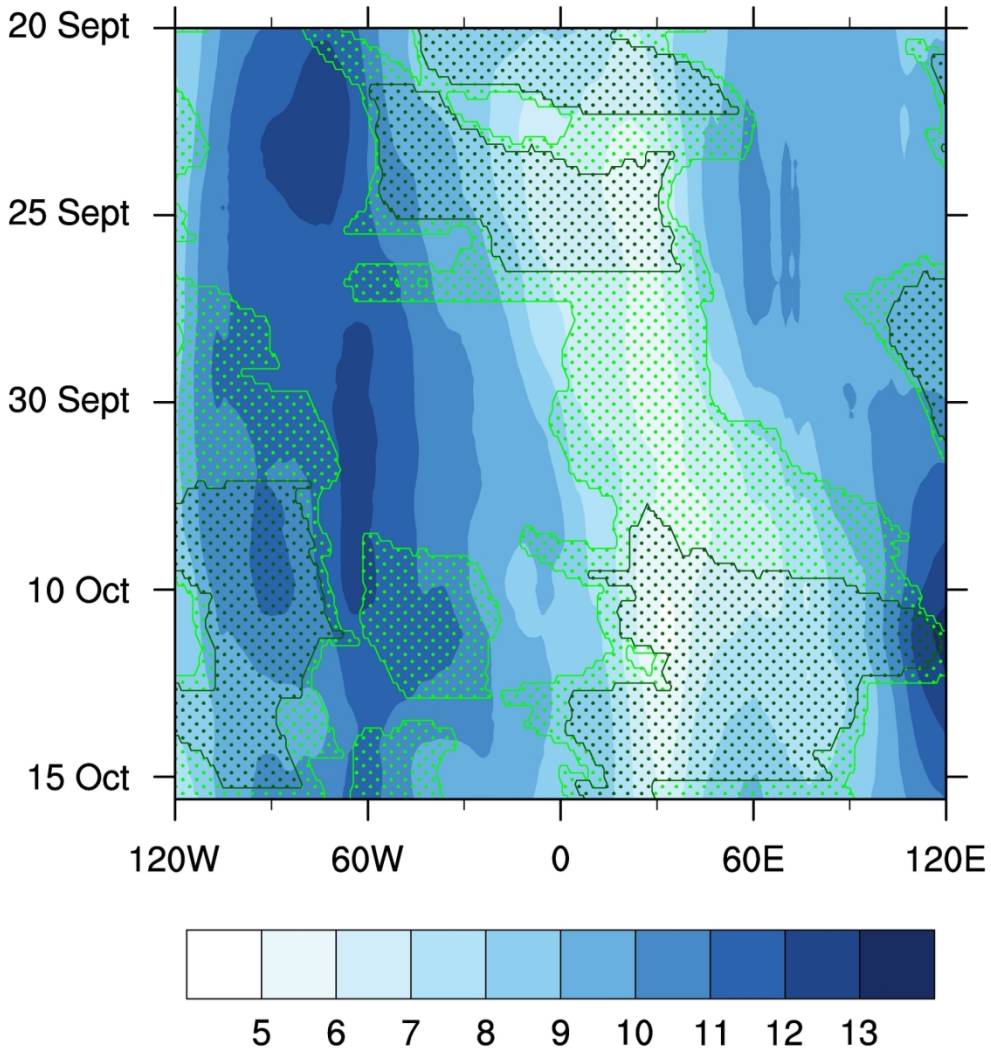

Figure 13. Evolution of meridionally averaged (30-80°N) low frequency (10-days running mean) zonal wind in 500hPa from 20 September 2000 to 15 October 2000. The darkgreen (green) dashed regions indicate the presence of a strong (weak) block between 30°N and 80°N.

152x162mm (300 x 300 DPI)

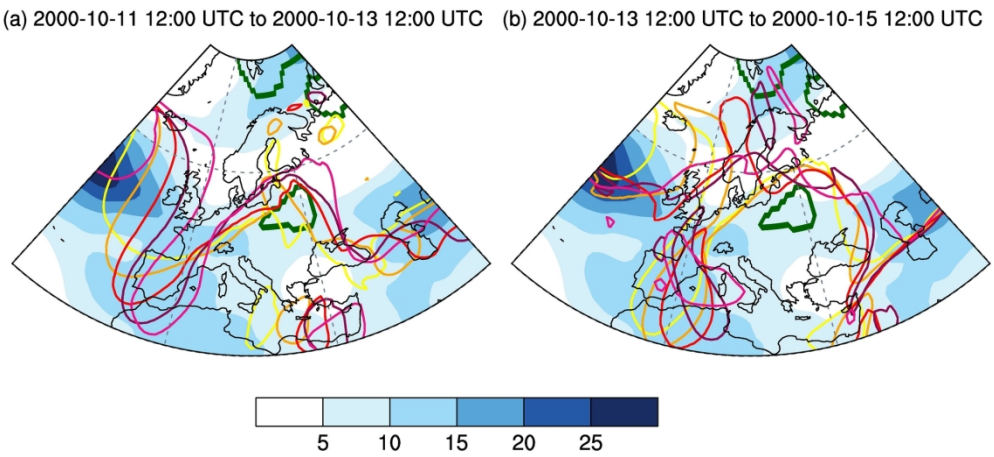

Figure 14. 10-days running mean of the zonal wind on 500hPa on 12 October 2000, 1200 UTC (a) and 14 October 2000 1200 UTC (b) (shading) and the position of the dynamical tropopause at 325K (contours) on 24h before (yellow), 12h before (orange), at the time (red) and 12h later (purple) and 24h later (pink). The green (darkgreen) indicates the location of the weak (strong) blocks.

174x81mm (300 x 300 DPI)